CHINA FOUNDRY Research & Development
Vol.13 No. 2 March 2016
DOI: 10.1007/s41230-016-5127-6

Modeling of aluminum-silicon irregular eutectic growth by cellular automaton model

Rui Chen, *Qing-yan Xu and Bai-cheng Liu

School of Materials Science and Engineering, Tsinghua University, Key Laboratory of Advanced Materials Processing Technology, MOE, Beijing 100084, China

Abstract: Due to the extensive application of Al-Si alloys in the automotive and aerospace industries as structural components, an understanding of their microstructural formation, such as dendrite and (Al+Si) eutectic, is of great importance to control the desirable microstructure, so as to modify the performance of castings. Since previous major themes of microstructural simulation are dendrite and regular eutectic growth, few efforts have been paid to simulate the irregular eutectic growth. Therefore, a multiphase cellular automaton (CA) model is developed and applied to simulate the time-dependent Al-Si irregular eutectic growth. Prior to model establishment, related experiments were carried out to investigate the influence of cooling rate and Sr modification on the growth of eutectic Si. This CA model incorporates several aspects, including growth algorithms and nucleation criterion, to achieve the competitive and cooperative growth mechanism for nonfaceted-faceted Al-Si irregular eutectic. The growth kinetics considers thermal undercooling, constitutional undercooling, and curvature undercooling, as well as the anisotropic characteristic of eutectic Si growth. The capturing rule takes into account the effects of modification on the silicon growth behaviors. The simulated results indicate that for unmodified alloy, the higher eutectic undercooling results in the higher eutectic growth velocity, and a more refined eutectic microstructure as well as narrower eutectic lamellar spacing. For modified alloy, the eutectic silicon tends to be obvious fibrous morphology and the morphology of eutectic Si is determined by both chemical modifier and cooling rate. The predicted microstructure of Al-7Si alloy under different solidification conditions shows that this proposed model can successfully reproduce both dendrite and eutectic microstructures.

Key words: Al-Si alloys; irregular eutectic growth; cellular automaton; modification; numerical simulation

CLC numbers: TG391.99 **Document code:** A **Article ID:** 1672-6421(2016)02-114-09

Due to an excellent combination of castability, high corrosion resistance and comprehensive mechanical properties, hypoeutectic Al-Si alloys are the most widely used commercial casting aluminum alloys which play an important role in the automotive and aerospace industries as structural components [1-4]. The typical as-cast microstructure of these alloys is mainly made up of primary dendrite and interdendrite (Al+Si) eutectic. Since the eutectic reaction usually occurs in the final stage of solidification, the eutectic growth behaviors, as well as eutectic silicon morphologies, distribution and volume fraction, remarkably affect the final castability, controlling the formation of casting defects, particularly porosity. Furthermore, the coarse, hard and brittle eutectic silicon phase in the softer eutectic aluminum phase also has a negative influence on the mechanical properties and heat-treatment response [5].

In order to improve the mechanical properties of Al-Si casting alloys, different approaches to control the eutectic microstructure, such as adding a chemical modifier to transform the coarse eutectic silicon to fibrous morphology or increasing the cooling rate to refine the eutectic structure, have been applied [6-8]. In the last decades, numerous experiments focusing on understanding the growth mechanism of modified Al-Si eutectic have been carried out, with various modification theories being proposed, among which the induced growth twinning theory is most universally accepted [9]. Insight into the nucleation characteristics both for modified and unmodified alloy have been investigated by Dahle et al.[10,11] through measuring the crystallographic orientation of eutectic aluminum in quenched samples and comparing with that of surrounding primary dendrites. However, the knowledge and quantitative understanding of eutectic formation in the final

*** Qing-yan Xu**

Male, born in 1971, Prof., Ph.D. His current research is interdisciplinary and focuses on a wide range of topics within the field of materials engineering, manufacturing process, mechanical engineering and integrated computational materials engineering (ICME). He is an author/co-author of over 150 peer-reviewed journal/conference papers, 5 edited books.

E-mail: scjxqy@tsinghua.edu.cn

Received: 2015-12-02; Accepted: 2016-01-15

solidification stage is still very limited, and further efforts need to be made to obtain a clear understanding of eutectic growth for different solidification conditions, thus to better control the solidified microstructures.

With the advancements of computer technology, numerical modeling and simulation for the solidification microstructure has become an important tool to enhance our physical understanding of time-dependent microstructural evolution. Nowadays, considerable progress has been made in modeling various aspects of solidification microstructure, and one of the major themes of research in this field is the numerical simulation of dendrite growth [12-15]. In parallel to the developments made in the field of dendrite growth, many efforts have also been devoted to the prediction of regular eutectic (nonfaceted-nonfaceted) growth by means of phase field or cellular automaton methods, and the regular eutectic morphologies have been reproduced successfully [16-19]. Recently, a few works have been carried out to make an attempt for the simulation of nonfaceted-faceted eutectic, mainly for Al-Si alloys [20,21]. Aiming at obtaining a deep insight into the (Al+Si) eutectic nucleation and growth behaviors, Zhu et al.[21] extended their previous modified cellular automaton model for describing dendrite growth and regular eutectic evolution to simulation of irregular eutectic alloy systems. The predicted Al-Si eutectic microstructure on morphology shows a good agreement with the experimental results given in the Ref. [10]. However, some of the parameters used in the previous simulations are lacking experimental evidence. Until now, the existing work on irregular eutectic simulation of Al-Si alloys is still far from satisfactory and further effort is still needed.

The objective of the present paper mainly focuses on the modelling and simulation of Al-Si irregular eutectic growth. Experiments to identify the influence of modification and cooling rate on eutectic microstructure are conducted prior to the mathematical model description. Based on the experimental results and analysis of the classical irregular eutectic growth theory, a cellular automaton model for irregular eutectic growth is presented by which some investigations on Al-Si eutectic growth behaviors are studied.

1 Experimental investigation

Commercial Al-7wt.%Si alloy was used in the current study. Prior to casting, the melting temperature was maintained at 720 °C and Sr modifier in the form of Al-10Sr master alloy was added into the melt. To obtain different cooling rates, the melt was poured into the sand mold with rod-shaped samples of different diameters (Φ: 40 mm, 24 mm, 12 mm and 7 mm). To record the temperature variation, a K-type thermocouple was embedded in the middle of each sample. Metallographic specimens were cut in the region near the thermocouple tips, and were observed with an optical microscope (OM) and a scanning electron microscope (SEM).

Figure 1 shows the measured cooling curves for five samples in order to illustrate the effects of Sr modification and cooling

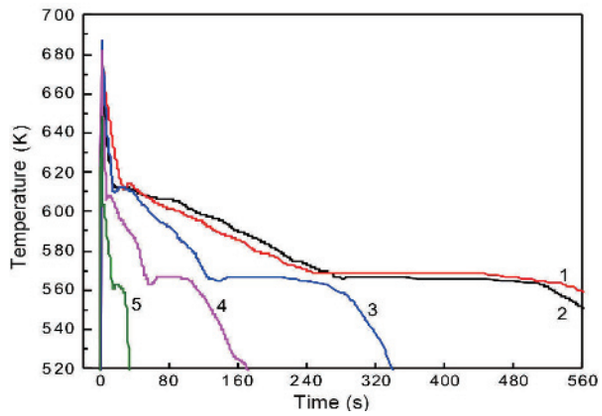

Fig. 1: Measured cooling curves for samples with different diameters

rate R_c on the eutectic temperature T_E, with the solidification conditions for each sample being displayed in Table 1. Through comparing sample 1 and sample 2, it can be seen that the addition of Sr modifier can shift the eutectic temperature to a lower value, resulting in a greater undercooling for eutectic solidification which can be described as $\Delta T_E = T_0 - T_E$ (T_0 is the equilibrium eutectic temperature equal to 574.6 °C calculated by Pandat). The eutectic undercooling for sample 1 is 7.0 K while it rises to 8.5 K for sample 2 which is Sr modified. For the modified sample 2 through sample 5, the eutectic temperature decreases from 566.1 to 560.1 °C as the cooling rate increases. The results agree well with other reports [8,22] in which Sr modification or a high cooling rate is accompanied by a depression in eutectic temperature. Figure 2 exhibits two typical modified and unmodified eutectic silicon morphologies. The morphology in Fig. 2(a) for unmodified sample 1 in slow cooled condition appears as coarse lamellar structure while it transforms to fibrous appearance for Sr-modified sample 5 at high cooling rate as shown in Fig. 2(b).

Table 1: Size and solidification conditions for each sample

No.	Φ (mm)	R_c (K•s^{-1})	T_E (K)	ΔT_E (K)	
Sample 1	40	0.4	567.6	7.0	unmodified
Sample 2	40	0.4	566.1	8.5	modified
Sample 3	24	0.7	564.6	10	modified
Sample 4	12	1.0	562.1	12.5	modified
Sample 5	7	4.0	560.1	14.5	modified

An interesting phenomenon was observed in our experiment that the average Si solubility in unmodified eutectic silicon for different cooling rates changes little and is approximately maintained at 93wt.%–97wt.%. For the modified alloy, however, the Si solubility decreases from 87wt.% to 70wt.% as the eutectic undercooling increases from 10 K to 14.5 K, which is displayed in Fig. 3. This phenomenon might result from the fact that Sr would segregate ahead of the growing interface, restricting the

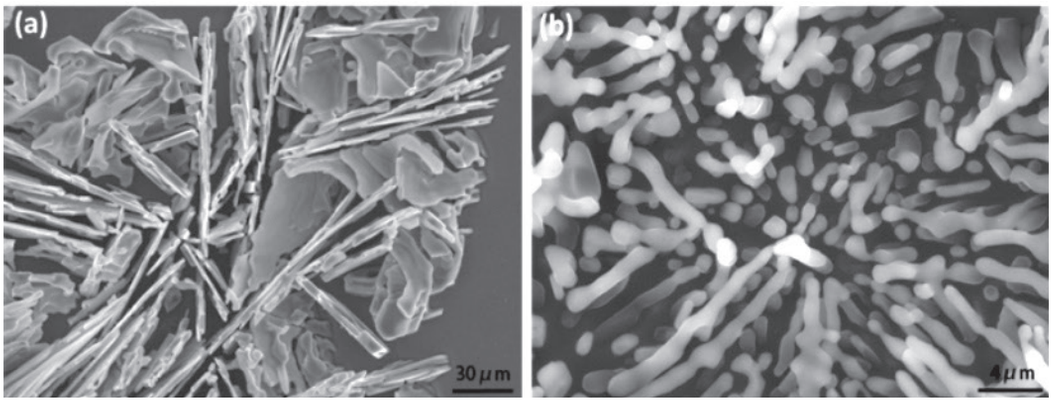

Fig. 2: Typical SEM micrographs of eutectic silicon morphologies for Al-7Si alloy: (a) Sample 1 and (b) Sample 5

diffusion of silicon in the melt [23]. Since the significant variation of Si solubility in eutectic silicon will have an influence on the eutectic growth as well as the volume fraction of eutectic silicon, it should be taken into account in simulations.

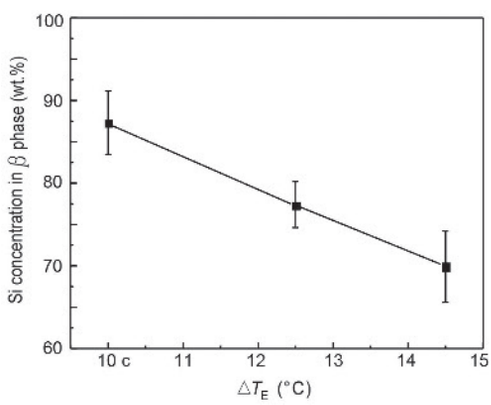

Fig. 3: Si concentration in eutectic silicon as a function of eutectic undercooling for modified alloy

2 Model description and numerical algorithms

It is known that Al-Si eutectic system is nonfaceted-faceted and the faceted Si (β phase) embeds in the nonfaceted eutectic Al matrix (α phase) as shown in Fig. 4. In the unmodified condition, the β phase tends to grow along certain directions so that the neighboring unaligned lamellar eutectic silicon will either diverge or converge with a large variation in lamellar spacing λ. When two lamellas converge, the spacing between them decreases as solidification proceeds and the growth of one will stop when the value of λ is less than a critical spacing λ_{min}. For diverging lamellas, if the spacing exceeds the maximum value λ_{max}, the growth becomes unstable and branching or nucleation occurs, thereby reducing the spacing. When Sr is added, the eutectic silicon is modified to fibers as seen in Fig. 2, which may result from the factors affecting the eutectic nucleation and growth behaviors. The impurity induced twinning theory for eutectic modification proposed by Hu and Hellawell [9] is widely accepted. It suggests that the impurity Sr adsorbs on the twin

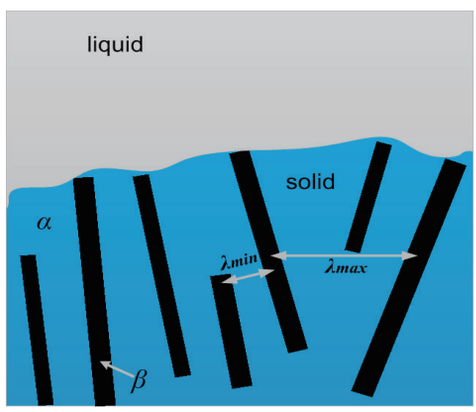

Fig. 4: Schematic of (Al+Si) irregular eutectic growth as well as the extremum lamellar spacing

plane re-entrant edge and retards the subsequent attachment of Si atoms, leading to more frequent overgrowth by α phase as well as greater ease for eutectic silicon to switch their growth directions. These experimental results and classical theories for (Al+Si) eutectic provide the basis for the following model establishment to describe the nucleation and growth behavior.

2.1 Solute diffusion calculation

Solute diffusion plays an important role in determining eutectic growth. For equilibrium solidification, the eutectic concentration is 12.6wt%, and the solubility of Si in α phase is 1.6wt% while the solubility of Si in β phase is close to 100wt%. Therefore, the growth of α phase will reject excess Si solute to its neighboring liquid cells and the growth of β phase will absorb Si element from surrounding liquid cells. Without considering natural and forced convection, the governing equation for solute diffusion within the entire domain is given by:

$$\frac{\partial w_\phi}{\partial t} = D_\phi \nabla^2 w_\phi + (w_\alpha - w_{\alpha 0})\frac{\partial f_{S,\alpha}}{\partial t} + (w_\beta - w_{\beta 0})\frac{\partial f_{S,\beta}}{\partial t} \quad (1)$$

where w is the composition with a subscript ϕ denoting the liquid, α phase or β phase. D_ϕ is the solute diffusion coefficient in ϕ phase. $w_{\alpha 0}$ and $w_{\beta 0}$ are the solubility of Si element in α phase and β phase, respectively. $f_{S,\alpha}$ and $f_{S,\beta}$ represent the solid

fraction. The secondary term and third term on the right hand of Eq.1 denote the amounts of solute rejected ($w_{\alpha 0}<w_{\phi}$) or absorbed ($w_{\beta 0}>w_{\phi}$) in interfacial cells due to the increment of solid fraction. The diffusion flux across α/β interface is assumed to be zero which means no diffusion across α/β interface. It has been pointed out in Fig. 3 that the eutectic undercooling, i.e., ΔT_E, has a significant effect on the solubility in β phase, i.e., $w_{\beta 0}$. Therefore, the value of $w_{\beta 0}$ used in simulations is obtained from the experimental data.

2.2 Growth kinetics and capture algorithm

Once the temperature of the melt reaches the eutectic temperature, eutectic reaction is triggered. The growth kinetics of Al-Si eutectic is determined by the local undercooling as described in Ref.[25]. In the present paper, the local undercooling $\Delta T(t_n)$ of an interfacial cell consists of thermal, constitutional and curvature effects which are characterized by the following equation:

$$\Delta T(t_n) = \Delta T_E + m_i\left[w(t_n) - w'_E\right] - \Gamma_i \overline{K}_i(t_n) \quad (2)$$

where m_i is the liquidus slope (i refers to α phase or β phase), which is negative for α phase and positive for β phase. $w(t_n)$ and $K_i(t_n)$ are the Si concentration and the mean curvature of an interfacial cell at the certain time t_n. Γ_i is the Gibbs-Thomson coefficient of i phase. As shown in Fig. 5, a decrease in the eutectic temperature will lead to the eutectic concentration shifting to a higher silicon content. In equilibrium, the eutectic is indicated as w_E, while it is $w_{'E}$ with a eutectic undercooling ΔT_E for metastable conditions. Hence, the variation in eutectic point should be considered in Eq. 2. The interface curvature of a cell with solid fraction f_S ($0<f_S<1$) is approximated by using the counting method with the expression given by:

$$\overline{K}_i(t_n) = \left[1 - 2\left(f_{S,i} + \sum_{j=1}^{N} f_{S,i}^{j}\right) \Big/ (N+1)\right] / \Delta x \quad (3)$$

where $f_{S,i}$ and $f_{S,i}^{j}$ are respectively corresponding to the solid fraction of i phase in the interfacial cell and its neighboring cells, and the number of N is equal to 8. Δx is the cell size. With the undercooling in Eq. 2 being calculated, the growth velocities $v(t_n)$ at time t_n both for eutectic α phase and silicon β phase can be analytically expressed as [26]:

$$v(t_n) = a \cdot \left[\Delta T(t_n)\right]^2 \quad (4)$$

where a is the growth kinetic coefficient whose value is determined to be 2.9 ($\mu m \cdot s^{-1} K^{-2}$) for nonfaceted α phase while it is 5.8 ($\mu m \cdot s^{-1} K^{-2}$) for faceted β phase. For a given interfacial cell, with the migration of the interface, the growth distance in every time step is transformed into the increment of solid fraction, and that is calculated separately for α phase and β phase by:

$$\Delta f_{S,\alpha} = v(t_n) \cdot \Delta t_n / \Delta x \quad (5)$$

$$\Delta f_{S,\beta} = \cos\theta \cdot v(t_n) \cdot \Delta t_n / \Delta x \quad (6)$$

where θ denotes the angle between the preferential growth direction and the linking line which is between the interfacial cell and the position of nucleus of β phase. This term $\cos\theta$ induces the effects of the deviation degree of the interfacial cell position from the preferential growth direction on the solid fraction increment, which agrees with the fact that for faceted eutectic silicon, the growth velocity along the preferential growth direction is much faster than other directions. Once the solid fraction of the interfacial cell exceeds unity, capturing neighboring liquid cells into interface begins. The capturing rule considers the growth behaviors of faceted β phase with or without modification. For unmodified silicon, the angle between the preferential growth direction and the linking line between the liquid cell and the position of nucleus of β phase is calculated. The liquid cell which occupies the lesser value tends to be more easily captured into the interface. According to Lu and Hellawell theory [9], in the presence of Sr modifier, the adsorption of Sr preferentially takes place on the twin re-entrant groove, forcing the silicon crystals to twin easily and increasing the ability to switch their growth directions. Results in Ref. [27] has confirmed that unmodified silicon structure has little twins, but the addition of modifier Sr significantly increases the density of twins. Hence, the capturing rule for modified silicon is different from the unmodified silicon in the model, which is mainly reflected in the increased possibility in multiple directions and decreased directivity in capturing.

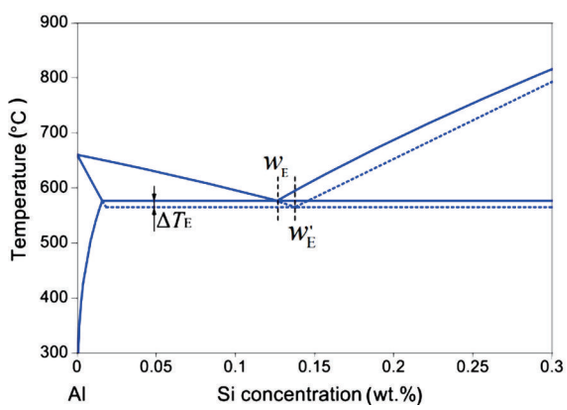

Fig. 5: Equilibrium phase diagram for Al-Si system with metastable extensions

2.3 Nucleation criterion

An understanding of nucleation mechanism is the prerequisite to describe the eutectic microstructural evolution. In past decades, the nucleation of Al-Si eutectic had been experimentally investigated [10-12,25,28]. It had been suggested that in unmodified alloys, the eutectic tends to nucleate on the tips of primary dendrite arms while the modified eutectic nuclei were found within the interdendritic liquid regions. Hence, the difference in nucleation position should be taken into account. The solute buildup or depletion ahead of eutectic phases will induce the potential nucleation sites. A nucleation criterion is introduced on the basis of the method generally used in the regular eutectic simulation in Refs.[18,19] . For L/α interfacial cell, if the solute concentration exceeds a critical value, i.e. $w_{L\alpha} - w'_E > \Delta w_\alpha$,

the cell is turned into L/β interface. Similarity, if the solute concentration of L/β interfacial cell is below a critical value, i.e., $w_{L\beta}-w'_E<\Delta w_\beta$, the L/$\beta$ interfacial cell transforms into L/α interface. This nucleation criterion is also similar to Qin's work [20], in which the driving force for Al-Si eutectic nucleation monotonously increasing with the deviation degree of solute concentration away from the equilibrium concentration is applied in their phase field model. In this study, the values of Δw_α and Δw_β were chosen to be 0.8 and –1.8, respectively. With the alternative nucleation of α phase and β phase in eutectic grains, competitive and coupling growth behavior is maintained.

3 Simulation results and discussion

To illustrate the capabilities of the proposed model, solidification process both for Al-Si eutectic alloys and Al-7Si alloy with or without Sr modification were simulated. The corresponding parameters used in the simulations are listed in Table 2, some of which are varying with the solidification conditions.

Table 2: Parameters used in the simulations [29]. "Exp" means the value depends on the solidification conditions

Definition and symbol (units)	Value
Eutectic temperature T_E (°C)	Exp
Eutectic concentration w'_E (wt.%)	Exp
Solubility in α phase $w_{\alpha 0}$ (wt.%)	1.65
Solubility in β phase $w_{\beta 0}$ (wt.%)	Exp
Liquid slope m_α (°C/wt.%)	-7.5
Liquid slope m_β (°C/wt.%)	17.5
Diffusion coefficient in liquid D_L ($m^2 \cdot s^{-1}$)	2.4×10^{-9}
Diffusion coefficient in solid D_S ($m^2 \cdot s^{-1}$)	3.0×10^{-12}
Gibbs-Thomson coefficient of α phase Γ_α (m•K)	1.96×10^{-7}
Gibbs-Thomson coefficient of β phase Γ_β (m•K)	1.7×10^{-7}

3.1 Unmodified irregular eutectic growth under different undercooling conditions

To provide an investigation on the irregular eutectic growth in unmodified Al-Si eutectic alloys, simulations were carried out in a domain containing 300×300 cells with a cell size of 1 μm. No mass flux conditions were imposed at the boundaries of the calculation domain, which was described by $\partial w_{\phi,i}/\partial n=0$. Various constant eutectic undercooling in the range of 4 K to 9 K was used for simulations, and the temperature was assumed to be uniform. The initial liquid concentration varied with the eutectic undercooling and was calculated from the metastable extentsions in Fig. 5, which can be expressed by an equation such as $w'_E=(T_E+83.5)/6.61$. At the beginning of simulation, a certain number of eutectic nuclei were randomly assigned in the calculation domain and each nucleus was generated by two neighboring liquid cells. One cell is the nonfacet α crystal and the other is the facet β crystal. Figure 6 shows the simulated eutectic growth sequences as well as the final eutectic morphologies at different eutectic undercooling conditions. The dark color in the figure represents the eutectic silicon, i.e., β phase, grey color for the liquid and white for the eutectic

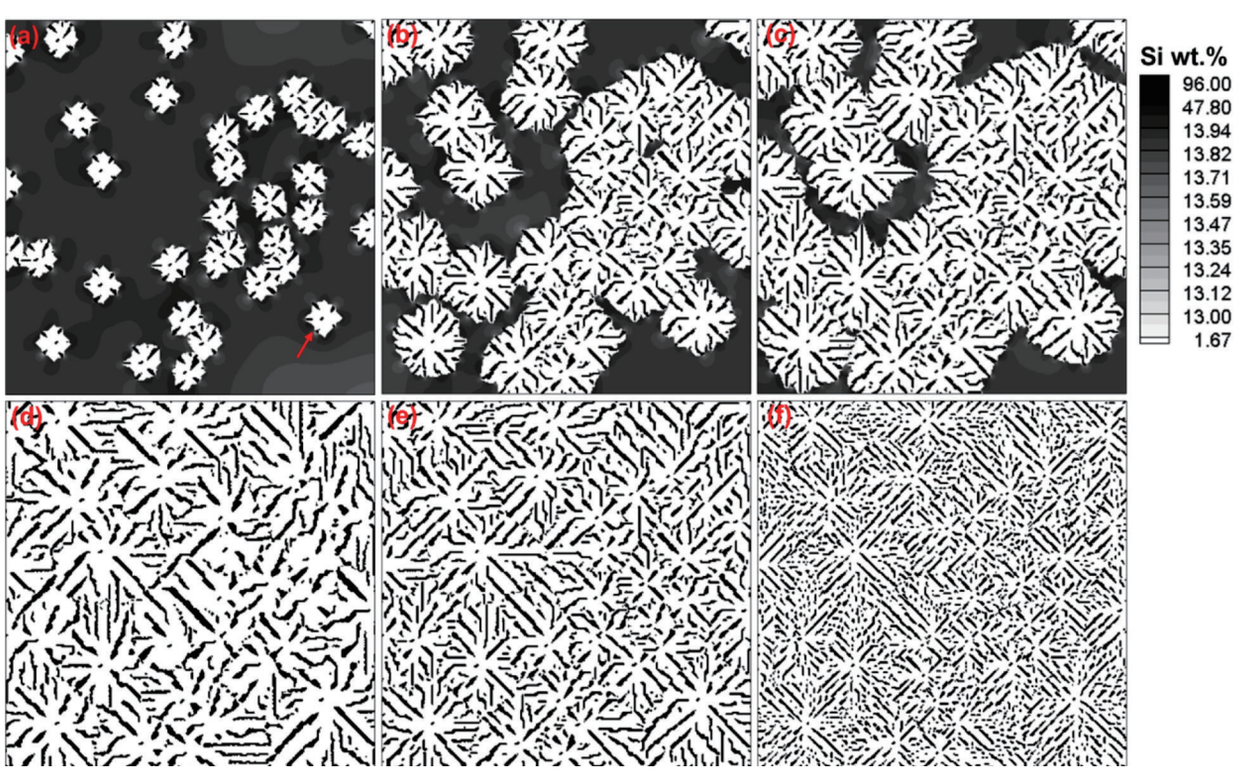

Fig. 6: Simulated results of unmodified (Al+Si) eutectic isothermally solidified with a eutectic undercooling ΔT_E = 6 K for various times: (a) 0.47 s, (b) 1.0 s, (c) 1.27 s. Eutectic morphologies under different eutectic undercooling conditions: (d) ΔT_E = 4 K, (e) ΔT_E = 6 K, (f) ΔT_E = 9 K

aluminum, i.e., α phase. It can be seen that the eutectic grains have a roughly spherical interface and the eutectic silicon tends to be suppressed or over-grown by the faster growing eutectic aluminum, resulting in the randomly distributed lamellar eutectic silicon, both of these phenomenon are consistent with those observed in experiments [22,26]. During the eutectic grains' growth process, the growth of α phase will reject excess solute as a result of solute redistribution while the growth of β phase will absorb amounts of solute from the surrounding liquid. Hence, the solute distribution in the liquid is non-uniform with the region of solute enriched existing ahead of α phase, and the region of solute depleted existing ahead of β phase as seen in Fig. 6(a-c). If the difference in solute distribution ahead of α or β phase exceeds the defined nucleation limit, nucleation of another phase will occur, leading to the competitive and cooperative growth pattern for α phase and β phase.

Figure 6(d-f) shows the influence of eutectic undercooling on eutectic growth, and it can be seen that an increase in eutectic undercooling will result in finer eutectic microstructure. Figure 7(a) displays the velocity profile of the eutectic grain indicated by the arrow in Fig. 6(a) as a function of solidification time. It can be seen that the growth velocity starts from a high value in the initial stage of solidification due to the imposed eutectic undercooling ΔT_E, and then it declines rapidly until to a relative stable value, approximately equal to 23 μm·s^{-1}.

Figure 7(b) shows the eutectic grain growth velocity as a function of ΔT_E. As expected, the growth velocity increases with the increasing of eutectic undercooling. The variation of growth velocity will affect the eutectic growth behavior. At a relatively low undercooling with a slow eutectic growth velocity [Fig. 6(d)], more time is available for the solute to diffuse out ahead of α phase and to be absorbed for the growth of β phase, decreasing the deviation of the solute concentration away from the eutectic composition w_E and lowering the possibility of nucleation. Under the condition of a high undercooling [Fig. 6(f)], the insufficient solute diffusion at the solidification front makes it more easier to reach the defined nucleation limit for both phases. Thus, alternative nucleation events occurring ahead of both phases eventually result in the discontinuous and finer lamellar eutectic microstructure, which can be characterized by the silicon lamellar spacing λ. In Ref. [30], it has been reported that lamellar spacing λ has an inverse relationship with the growth velocity of eutectic interface v, i.e., $\lambda^2 v$ = C, in which C is constant. This analytical expression is consistent with the simulated results in Fig. 8 that a higher growth velocity corresponds to a higher eutectic undercooling, and tends to refine the eutectic microstructure and narrow the eutectic lamellar spacing.

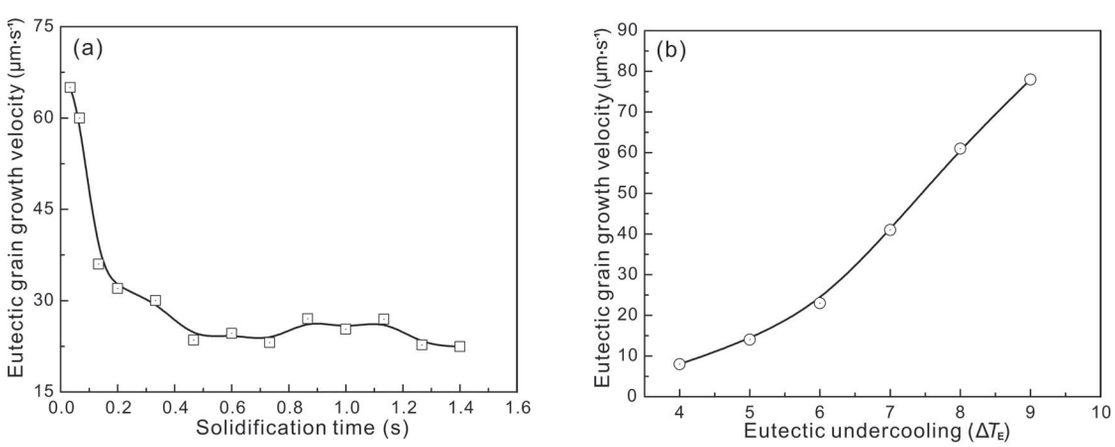

Fig. 7: Growth velocity of eutectic grain as a function of solidification time at ΔT_E=6 K (a) and growth velocity of eutectic grain in steady state as a function of eutectic undercooling (b)

3.2 Effects of Sr modification on the eutectic growth

In this section, the proposed CA model was applied to simulate the modified eutectic growth and the influence of eutectic undercooling was investigated. The eutectic concentrations were obtained from the metastable extensions in Fig. 5, that is w'_E=14.1wt.% at ΔT_E=10 K and w'_E=14.8wt.% at ΔT_E=14.5 K. The calculation domain having 200×200 cells with a cell size of 1 μm was chosen. The simulated results are shown in Fig. 8, with figure (a-b) denoting the microstructure at different times at ΔT_E=10 K, and figure (c) being the eutectic microstructure at ΔT_E=14.5 K. The competitive and cooperative growth mode with spherical appearance of eutectic grains is visibly similar to that of unmodified alloy indicated in Fig. 6, while the modified eutectic silicon tends toward easier nucleation and switching growth directions, being consistent with Hu and Hellawell's theory. It can also be found by comparing Fig. 8(b) with Fig. 8(c) that an increase in eutectic undercooling will result in a finer eutectic silicon with a more obvious fibrous morphology. Since eutectic undercooling is affected by the cooling rate and modification, only when both the chemical modifier and the high cooling rate are imposed, can the fully modified eutectic structure be obtained.

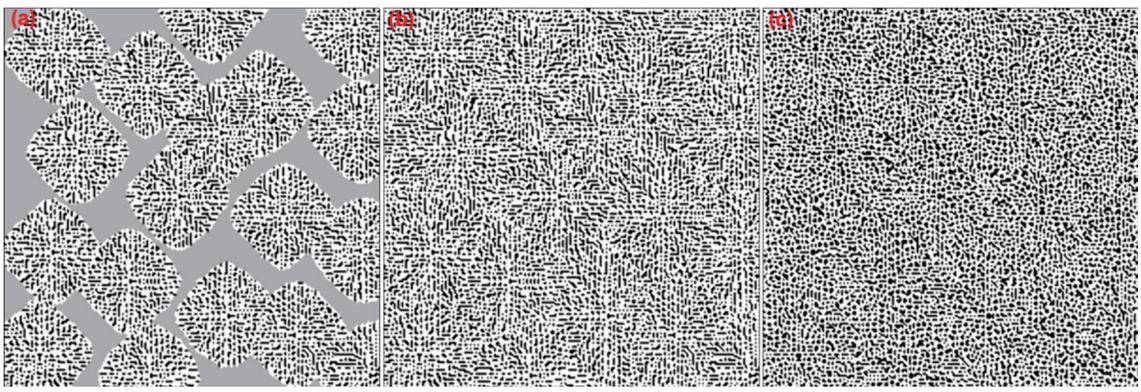

Fig. 8: Simulated microstructural evolution of modified eutectic isothermally solidified at ΔT_E=10 K for various times: (a) 0.23 s, (b) 0.44 s, (c) Simulated modified eutectic microstructure at ΔT_E=14.5 K

3.3 Simulation of dendrite and eutectic growth in unmodified and modified Al-7wt.%Si alloy

For hypoeutectic Al-7wt.%Si alloy, the first solid phase formation is primary α-Al dendrite, followed by (α-Al+β-Si) eutectic. It is known that dendrite microstructure is influenced by cooling conditions. The higher the cooling ratμm•$s^{-1}K^{-2}$e, the finer the dendrite microstructure, with more and narrower interdendritic regions separated by the grain boundaries, in which the solute is substantially enriched and eutectic reaction would take place. Furthermore, the higher cooling rate will decrease the eutectic temperature, resulting in a higher undercooling for eutectic growth as well as higher solubility of Si atoms in eutectic silicon. Hence, the eutectic growth behavior within the interdendritic regions is expected to be influenced by the cooling rate. The influence of the cooling rate on both dendrite and eutectic formation is investigated in this section. Three kinds of simulation conditions corresponding to sample 1, sample 4 and sample 5 as shown in Table 1 were performed. The parameters w'_E and $w_{\beta 0}$ were obtained from the metastable extensions in Fig. 5 and experimental results in Fig. 3. The calculation domain consists of 600×600 cells with a cell size of 1 μm. The temperature field in the calculation domain is assumed to be uniform with a constant cooling rate R_c for dendrite growth, and a certain number of dendrite nuclei with random preferential growth orientations is originally placed in the domain. Figure 9 displays the simulated dendrite and eutectic microstructure, and it can be clearly observed that a low cooling rate for the unmodified alloy results in the coarse dendrite microstructure as well as lamellar eutectic silicon morphologies, as shown in Fig. 9(a). When the cooling rate is increased and Sr is added, both the dendrite and eutectic is refined and the eutectic silicon is transformed to fibrous [Fig. 9(b,c)]. This phenomenon can be more clearly seen in Fig.10 where the comparison between simulated and experimental results is depicted. This indicates that the present CA model can reproduce both dendrite and eutectic microstructures realistically and can be used to investigate the effects of solidification conditions on microstructural evolution.

Table 3 illustrates the influence of cooling conditions on the evolution of microstructure volume fractions. As can be seen, the higher cooling rate results in the lower dendrite volume fraction and higher fractions both for eutectic α phase and β phase, which is consistent with that in Ref.[31]. Under slow cooling conditions, more time is available for solute diffusion with lower solute enrichment within the liquid, resulting in a higher volume fraction of primary phase, which in turn contributes to the lower eutectic volume fraction. The decreased

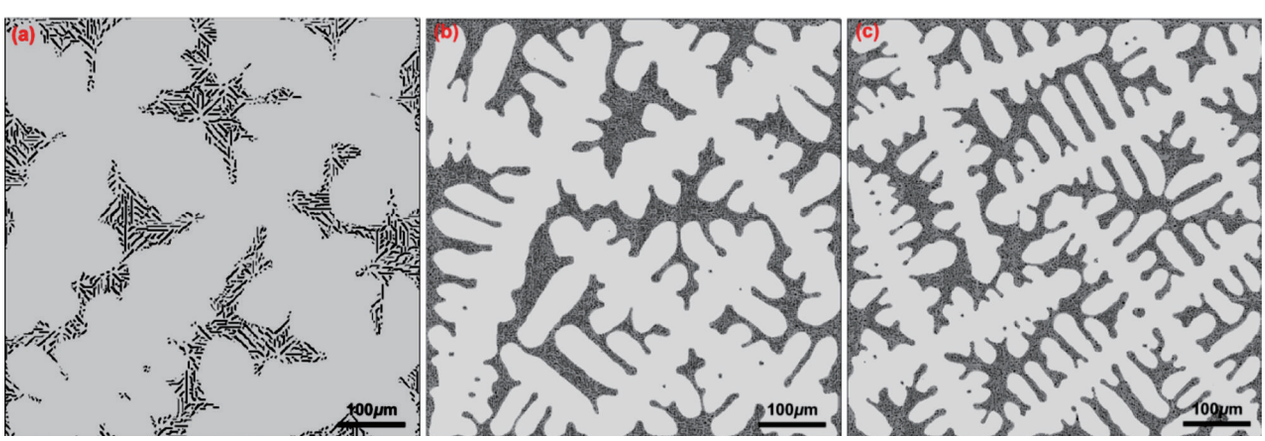

Fig. 9: Dendrite growth coupled with eutectic formation under different solidification conditions: (a) sample 1, (b) sample 4, (c) sample 5

Table 3: Simulated volume fractions of primary *α*-Al phase, eutectic *α* phase, eutectic *β* phase under different cooling conditions

No.	Primary *α*-Al (%)	Eutectic *α* (%)	Eutectic *β* (%)
Sample 1	70.9	23.9	5.2
Sample 4	67.5	26.8	5.7
Sample 5	65.5	28.2	6.3

solubility of Si in eutectic silicon with the increasing of eutectic undercooling also contributes to the incremental increase in the volume fraction of *β* phase.

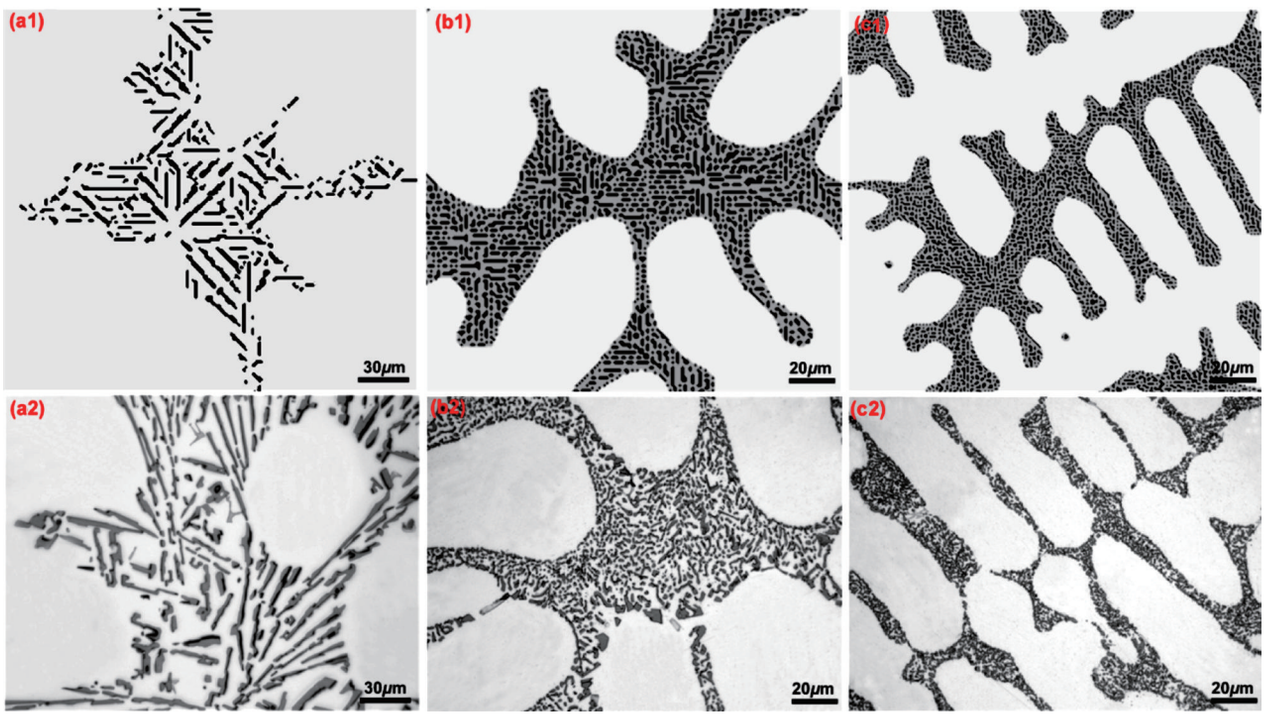

Fig. 10: Comparison of simulated and experimental microstructures: (a1, a2) simulated and experimental results for sample 1; (b1, b2) simulated and experimental results for sample 4; (c1, c2) simulated and experimental results for sample 5; (a1-c1) is the local view in Fig. 9(a-c)

4 Conclusions

Experimental investigation on (Al+Si) irregular eutectic growth in Al-7Si alloy was carried out. The parameters including eutectic undercooling and Si solubility in eutectic silicon under different solidification conditions were investigated. It was found that high cooling rate and Sr modification tend to depress the eutectic temperature, and the solubility of Si atoms in eutectic silicon varies significantly with the cooling rate for modified alloy.

A multiphase CA model was proposed with the advantage of describing the time-dependent Al-Si eutectic growth. This model incorporates several aspects including growth algorithms and nucleation criterion to achieve the competitive and cooperative growth mechanism for nonfaceted-faceted Al-Si irregular eutectic. The capturing rule considers the effects of modification on the growth behaviors of faceted *β* phase.

The simulated results reveal that for unmodified alloy, a high eutectic undercooling can refine the eutectic microstructure and narrow the eutectic lamellar spacing. When the melt is modified by Sr, the alternative nucleation tends to be easier, with the eutectic silicon being obvious fibrous morphology. The modification effects are closely related to the cooling rate, revealing that only when both the chemical modifier and high cooling rater are imposed, can the fuly modified eutectic structure be obtained. Finally, the microstructural evolution of Al-7Si alloy under different solidification conditions was simulated, and the predicted and experimental microstructure shows a good agreement, indicating that this model can successfully reproduce both dendrite and eutectic microstructures.

References

[1] Li P T, Liu S D, Zhang L L, et al. Grain refinement of A356 alloy by Al-Ti-B-C master alloy and its effect on mechanical properties. Materials and Design, 2013, 47: 522–528.

[2] Zhu M, Jian Z Y, Yang G C, et al. Effects of T6 heat treatment on the microstructure, tensile properties, and fracture behavior of the modified A356 alloys. Materials and Design, 2012, 36: 243–249.

[3] Liao H C, Zhang M, Bi J J, et al. Eutectic solidification in near-eutectic Al-Si casting alloys. Journal of Materials Science & Technology, 2010, 26: 1089–1097.

[4] Abedi A, Shahmiri M, Amir Esgandari B, et al. Microstructure evolution during partial remelting of Al-Si alloys containing different amounts of magnesium. Journal of Materials Science & Technology, 2013, 29: 971–978.

[5] Knuutinen A, Nogita K, McDonald S D, et al. Modification of Al-Si alloys with Ba, Ca, Y and Yb. Journal of Light Metals, 2001, 1: 229–240.
[6] Hosch T, England L G and Napolitano R E. Analysis of the high growth-rate transition in AL-Si eutectic solidification. Journal of Materials Science, 2009, 44: 4892–4899.
[7] Li B, Huang H W, Jie J C, et al. Effects of yttrium and heat treatment on the microstructure and tensile properties of Al-7.5Si-0.5Mg alloy. Materials and Design, 2011, 32: 1617–1622.
[8] Chen X, Geng H Y and Li Y X. Study on the eutectic modification level of Al-7Si alloy by computer aided recognition of thermal analysis cooling curves. Materials Science and Engineering A, 2006, 419: 283–289.
[9] Lu S and Hellawell A. Growth mechanisms of silicon in Al-Si alloys. Journal of Crystal growth, 1985, 73: 316–328.
[10] Dahle A K, Nogita K, Zindel J W, et al. Eutectic nucleation and growth in hypoeutectic Al-Si alloys at different strontium levels. Metallurgical and Materials Transactions A, 2001, 32: 949–960.
[11] Nogita K, Knuutinen A, McDonald S D, et al. Mechanisms of eutectic solidification in Al-Si alloy modified with Ba, Ca, Y and Yb. Journal of Light Metals, 2001, 1: 219–228.
[12] Du Q and Jacot A. A two-dimensional microsegregation model for the description of microstructure formation during solidification in multicomponent alloys: Formulation and behaviour of the model. Acta Materialia, 2005, 53: 3479–3493.
[13] Zhu M F and Stefanescu D M. Virtual front tracking model for the quantitative modeling of dendritic growth in solidification of alloys. Acta Materialia, 2007, 55: 1741–1755.
[14] Shi Y F, Xu Q Y, Gong M, et al. Simulation of NH4Cl-H2O dendritic growth in directional solidification. Acta Metallurgica Sinica, 2011, 47: 620–627. (In Chinese)
[15] Böttger B, Eiken J and Steinbach I. Phase field simulation of equiaxed solidification in technical alloys. Acta Materialia, 2006, 54: 2697–2704.
[16] Yang Y J and Yan B. Three dimensional multi-phase field simulation of growth of eutectic CBr_4-C_2Cl_6 alloy Ⅰ: Modeling and Testing. Acta Metallurgica Sinica, 2010, 46: 781–786. (In Chinese)
[17] Shi Y F, Xu Q Y and Liu B C. Simulation of eutectic growth in directional solidification by cellular automaton method. Acta Metallurgica Sinica, 2012, 48: 41–48. (In Chinese)
[18] Zhu M F and Hong C P. Modeling of microstructure evolution in regular eutectic growth. Physical Review B, 2002, 66: 155428.
[19] Xiong S M and Wu M W. Experimental and modeling studies of the lamellar eutectic growth of Mg-Al alloy. Metallurgical and Materials Transactions A, 2012, 34: 208–218.
[20] Qin R S and Wallach E R. Computer simulation of the aluminium-silicon anomalous eutectic growth based on multiphase field method. Materials Transactions, 2003, 44: 968–972.
[21] Zhu M F and Hong C P. Modeling of irregular eutectic microstructure in solidification of Al-Si alloys. Metallurgical and Materials Transactions A, 2004, 35: 1555–1563.
[22] McDonald S D, Nogita K and Dahle A K. Eutectic nucleation in Al-Si alloys. Acta Materialia. 2004, 52: 4273–4280.
[23] Hegde S and Prabhu K.N. Modification of eutectic silicon in Al-Si alloys. Journal of Materials Science, 2008, 43: 3009–3027.
[24] Chen R, Xu Q Y and Liu B C. A modified cellular automaton model for the quantitative prediction of equiaxed and columnar dendritic growth. Journal of Materials Science Technology, 2014, 30: 1311–1320.
[25] McDonald S D, Dahle A K, Taylor J A, et al. Eutectic grains in unmodified and strontium-modified hypoeutectic aluminum-silicon alloys. Metallurgical and Materials Transactions A, 2004, 35: 1829–1837.
[26] Stefanescu D M, Upadhya G and Bandyopadhyay D. Heat transfer-solidification kinetics modeling of solidification of castings. Metallurgical Transactions A,1990, 21: 997–1005.
[27] Guthy H V. Evolution of the eutectic microstructure in chemically modified and unmodified aluminum silicon alloys [Dissertation], Worcester Polytechnic Institute, Massachusetts, 2002.
[28] Nafisi S, Ghomashchi R and Vali H. Eutectic nucleation in hypoeutectic Al-Si alloys. Materials Characterization, 2008, 59: 1466–1473.
[29] Gündüz M, Kaya H, Cadırlı E, et al. Interflake spacings and undercoolings in Al-Si irregular eutectic alloy. Materials Science and Engineering A, 2004, 369: 215–229.
[30] Fisher D J and Kurz W. A theory of branching limited growth of irregular eutectics. Acta Metallrugica, 1980, 28: 777–794.
[31] Chen R, Shi Y F, Xu Q Y, et al. Effect of cooling rate on solidification parameters and microstructure of Al-7Si-0.3Mg-0.15Fe alloy. Transaction of Nonferrous Metals Society of China, 2014, 24: 1645–1652.

The study was financially supported by the National Basic Research Program of China (Grant No. 2011CB706801), the National Natural Science Foundation of China (Grant No. 51374137, 51171089), and the National Science and Technology Major Projects (Grant No. 2012ZX04012-011, 2011ZX04014-052).